Raman spectra of solid isotopic hydrogen mixtures

B. J. Kozioziemski and G. W. Collins
Lawrence Livermore National Laboratory, Livermore, California 94551
(Received 13 November 2002; published 1 May 2003)

Rotational and vibrational Raman spectra are investigated for mixtures of hydrogen isotopes in the solid phase. The $S_0(0)$ rotational Raman transitions are asymmetrically broadened in energy for each isotope in the mixture compared to their respective pure component transitions. The isotopic energy shift of $S_0(0)$ breaks the lattice symmetry and limits the roton hopping responsible for the well defined $S_0(0)$ triplet found in the pure component. The $S_0(0)$ line shapes of tritiated and nontritiated mixtures are nearly identical, and shows there is little effect from radiation damage. The vibrational $Q_1(J)$ lines are shifted to higher energy, and the $Q_1(1)/Q_1(0)$ intensity ratio is decreased in the mixtures relative to the pure component. Both effects are due to a localization of the vibrons in mixtures.

DOI: 10.1103/PhysRevB.67.174101 PACS number(s): 78.30.Hv, 33.20.Vq, 33.20.Fb

I. INTRODUCTION

Hydrogen forms a molecular quantum solid at low temperatures which has engaged a great deal of interest throughout the last century and continues today. The many research areas studied include anisotropic interactions,[1–4] matrix impurities,[5–7] rotational diffusion,[8] and pressure effects[9–11] on the rotational and vibrational Raman spectra.[8,12,13] Research continues to focus on hydrogen in high pressure and fusion energy research, both of which may use the Raman spectra as a diagnostic. The National Ignition Facility in particular will use an isotope mixture of 25%-50%-25% D_2-DT-T_2 (D-T) in high-gain fuel capsules.[14] The rotational Raman spectrum provides one measurement of the isotope concentrations in the fuel layer.[15,16,17] While the Raman spectra of single isotope hydrogen solids are well known, those of mixtures, particularly with tritium, have received less attention.

Properties of the hydrogen molecules in the zero-pressure solid are not too different from those of the free molecules.[8,13] The weak intermolecular interactions do not mix rotational energy states; hence the rotations are free and J is a good quantum number. $\Delta J=2$ is first allowed rotational transition for homonuclear molecules. The fivefold J = 2 degeneracy is lifted and the rotational states are broadened into an energy band by the crystal field interaction. Similarly, the molecular vibrational states are weakly perturbed by the intermolecular interactions, also forming a band in the solid. The rotational and vibrational Raman spectra probe the respective energy bands in the solid.

Radiation damage in D-T results from the beta decay of the triton.[18] The mean decay energy of 5.7 keV goes into ionization, dissociation, molecular excitations, and the heating of the solid. The free atoms created by the beta decay were shown to convert J = 1 molecules as the atoms rapidly hop through the lattice.[19–21] Hence, the J = 1-to-0 conversion proceeds much faster in D-T than in nontritiated hydrogens. The effect of radiation damage on the rotational and vibrational bands was studied using infrared spectroscopy,[22] but no work has yet explored the Raman spectrum. This paper shows that there is little change in the rotational and vibrational Raman spectra due to tritium radiation damage to the solid. However, the spectra of the mixtures do differ from those of the pure component hydrogens.

The notation of Souers[18] is followed in this paper, with any of the six diatomic combination of H, D, and T atoms referred to as hydrogen and referring to specific isotopic combinations when required, i.e., H_2, HD. H-D will refer to mixtures of H_2, D_2, and HD. The Raman spectrum for the rotational transitions $S_0(0)$ and $S_0(1)$ and the vibrational transitions $Q_1(0)$ and $Q_1(1)$ of hydrogen relevant to this paper are reviewed first. These results for pure hydrogens provide the basis for understanding the observed spectrum in mixtures. Sections III and IV compare mixtures of H-D and D-T with pure component samples.

A. Review of rotational Raman spectrum

Only the rotational J = 0 ground and J = 1 metastable states are populated in the low temperature and pressure solid hydrogens.[8,18] Neighboring J = 1 molecules in H_2, D_2, and T_2 solids interact via their magnetic dipoles (and electric quadrupoles for D_2) thus decoupling the nuclear spins and enabling conversion from the metastable J = 1 state to the J = 0 state.[13,23–25] The conversion rate is slow enough to permit treating J = 1 and J = 0 molecules as separate species. $c(J)$, the concentration of molecules in rotational state J, is determined from the $\Delta J=2$ allowed Raman transitions $S_0(0)$ and $S_0(1)$ of the homonuclear molecules as follows. The scattering intensity for $\Delta J=2$ is calculated to be proportional to the number of molecules in the initial rotational state J, $N(J)$, according to[15]

$$I_J \propto N(J)\frac{(J+1)(J+2)}{(2J+3)(2J+1)}\omega^4|\langle\psi|\alpha_J|\psi\rangle|^2. \qquad (1)$$

The anisotropic polarizability matrix elements $\langle\psi|\alpha_{J=0}|\psi\rangle$ and $\langle\psi|\alpha_{J=1}|\psi\rangle$ differ by less than 1% for H_2 molecules, while the H_2 and D_2 isotope polarizabilities differ by 4%.[26,27] Further, there is no phonon interaction because the rotational transition energies of the hydrogens are larger than their Debye temperatures. Hence, $N(1)/N(0)$ is obtained from the ratio of the scattering intensities I(J = 1-3)/I(J = 0-2) as[16]

$$\frac{N(J=1)}{N(J=0)}=\frac{5}{3}\frac{I(J=1-3)}{I(J=0-2)}. \tag{2}$$

The isotopic concentrations in hydrogen mixtures are obtained from the Raman intensities by scaling appropriately according to the anisotropic polarizabilities.[27] Thus, the rotational Raman spectrum provides the concentrations of the isotopes and rotational states.

The electric quadrupole-quadrupole (EQQ) and crystal field interactions in the solid couple hydrogen molecules and partially lift the degeneracy of the five m_J $S_0(0)$ transitions. The resulting Raman spectrum is a well defined triplet (doublet) for pure H_2 or D_2 with less than $c(1)$ = 5-10% in the hcp (fcc) lattice.[8,10,28] Both interactions are reviewed, since they provide a basis for understanding the Raman spectrum of hydrogen mixtures.

1. EQQ interaction

The EQQ interaction couples the J = 2 excitation to neighboring J = 0 molecules, enabling the excitation to hop through the lattice. A rotational exciton band results, with the allowed energies dependent on the lattice structure. Van Kranendonk provided a solution to both the fcc and hcp lattices using Bloch's theorem. The allowed energy states $E(\mathbf{k})$ with roton waqve function amplitude $A_m(\mathbf{k})$ of the hcp lattice are the solutions to the 10x10 secular equation [Eq. (4.43) in Ref. 8]

$$\sum_n H_{m,n}(\mathbf{k})A_n(\mathbf{k})=E(\mathbf{k})A_m(\mathbf{k}). \tag{3}$$

The fcc expression is similar and not presented here. The Hamiltonian matrix is defined as

$$H_{m,n}=\sum_j \langle 2m,R_i|V_{EQQ}|2n,R_j\rangle=\epsilon_{02}c_{mn}S_{n-m}, \tag{4}$$

where ϵ_{02} is the quadrupole coupling constant and $c_{mn}=\sqrt{70}(-1)^m C(224;m\bar{n})$ incorporates the Clebsch-Gordon coefficient. R_i is the position of the ith molecule. The lattice sums are expressed as

$$S_\mu=\sum_\rho \left(\frac{R_0}{R_\rho}\right)^5 C_{4\mu}(\Omega_\rho), \tag{5}$$

where $C_{4\mu}(\Omega)$ is the Racah spherical harmonic, R_ρ and Ω_ρ are the distance and angle to the molecular site ρ, and R_0 is the nearest neighbor separation. The point symmetry of the hcp lattice makes the lattice sum nonzero only when $\mu=0$. The approximation of $\mathbf{k}=0$ is made in Eq. (3) since the wave vector of the excitation is small compared to the lattice spacing. The eigenvalues of Eq. (3) are the five Raman allowed energy states that have three distinct energies, $0.903\epsilon_{02}a_m(4)$, where $a_{\pm1}=-4$, $a_{\pm2}=1$, and $a_0=6$, and the factor of 0.903 is the resulting value of the lattice sum.[8] Hence, the rotational spectrum in a hcp lattice consists of three equally spaced lines. The above derivation assumes a rigid lattice, with the details of phonon renormalization available.[8] Crystal field interactions modify the above energies as described below.

2. Crystal field terms

The crystal field terms are due to the interaction of the anisotropic potential of the J = 2 molecule with the isotropic part of the neighboring J = 0 molecules. The potential is expressed in the crystal reference frame with the z axis along the hexagonal c axis as[1]

$$V_c=\sum_{\substack{l=2,4\\ n=-l,l}} \epsilon_{ln}Y_{ln}(\omega), \tag{6}$$

where ω is the orientation of the molecule in the hcp lattice, Y_{ln} is the spherical harmonic, and the coupling constants are given by[1]

$$\epsilon_{ln}=\sum_i g(R_i)Y_{ln}^*(\alpha_i,\beta_i). \tag{7}$$

Here, $g(R_i)$ is the radial part of the potential, R_i, α_i and β_i refer to the coordinates of the central J = 2 molecule pointing to the neighboring J = 0 molecules, and the sum is over all molecules in the crystal. All of the $n\neq0$ terms are zero due to the point symmetry of the single component hcp lattice, and $|2m\rangle$ states are not mixed.

For any given configuration of H_2 or D_2 molecules in the lattice the crystal field energies can be calculated by diagonalizing the potential according to

$$E=\langle 2m|V_c|2m\rangle. \tag{8}$$

The sum in Eq. (7) drops off quickly with R_i and only the first few shells of neighbors need be considered. The solution for the crystal field energies are[29]

$$E_c(2m)=-\frac{2}{7}c_m\epsilon_{2c}+\frac{1}{21}a_m\epsilon_{4c}, \tag{9}$$

where a_m are as defined for the EQQ interaction and $c_{\pm2}=1$, $c_{\pm1}=-1/2$, $c_0=-1$. Hence, a non-zero ϵ_{2c} leads to unequal values of $\Delta_1=S_0(0)_{\pm2}-S_0(0)_{\pm1}$ and $\Delta_2=S_0(0)_0-S_0(0)_{\pm2}$. The measured difference of Δ_1 and Δ_2 originally measured by Bhatnagar[30] is 0.03 cm^{-1} for H_2, small compared to $\Delta_1=2.01$ cm^{-1}. This early measurement is consistent with more recent high resolution methods.[31,32] The ϵ_{4c} term has the same symmetry as the EQQ interaction, but is negative in sign.[29] Hence, the triplet spacing is reduced from the EQQ hopping calculation.

The above results are valid for hydrogens with $c(1)$ less than a few percent. The $S_0(0)$ line is broadened and the triplet is unresolvable above $c(1)=20\%$ in D_2.[30] In contrast, Hardy *et al.*[16] studied the rotational Raman spectrum of H_2 and D_2 with very low $c(0)$ in a J = 1 lattice. In this case, J = 0 molecules are the impurities. They found the $S_0(0)$ m_J energies, listed in Table I, were consistent with the $Pa3$ lattice symmetry for the the ordered lattice at 1.16 K, with an ordering of the m_J components that differs from the hcp lattice. However, the $S_0(0)$ line is broad and asymmetric in

TABLE I. Solid phase $S_0(0)$ energies. The first nine are measured in this work while the last four provide reference values. m_J are identified only when known.

Isotope	Composition	Position (cm^{-1})	FWHM (cm^{-1})	Splitting (cm^{-1})	%J=1	Temp. (K)
H_2	12%H_2-88%D_2	352.8	3.0		<5	8.5
		355.3	1.8	2.5		
		357.9	3.4	2.6		
D_2	100% D_2	$m_{\pm1}$=177.1	1.0		<1	12.5
		$m_{\pm2}$=179.6	1.0	2.5		
		m_0=182.1	1.0	2.5		
D_2	12%H_2-88%D_2	177.4	2.9		<5	8.5
		179.8	2.5	2.4		
		182.3	2.5	2.5		
D_2	23%H_2-77%D_2	177.4	4.1		<5	8.5
		180.0	3.8	2.6		
		182.3	3.8	2.3		
D_2	77%H_2-23%D_2	177.2	3.0		<5	9.2
		179.5	1.3	2.25		
		182.2	3.8	2.7		
D_2	46%H_2-38%HD-16%D_2	176.5	2.9		<5	7.5
		178.8	1.1	2.3		
		181.8	2.9	3.0		
D_2	29%H_2-51%HD-20%D_2	176.1	2.6		<5	8.0
		178.4	1.4	2.3		
		181.8	3.5	3.4		
D_2	D-T				<2	10.2
		CM - 178.8				
		peak - 176.8				
T_2	D-T	116.3	2.2		<2	10.2
		118.8	2.2	2.5		
		122.7	4.2	3.9		
H_2	100% H_2	$m_{\pm1}$=351.84	0.6		<1	2
(Bhatnagar *et al.*) (Ref. 30)		$m_{\pm2}$=353.85	0.6	2.01		
		m_0=355.83	0.6	1.98		
D_2	100% D_2	$m_{\pm1}$=176.8	2		20	2
(Bhatnagar *et al.*) (Ref. 30)		$m_{\pm2}$=179.4	2	2.6		
		m_0=182.0	2	2.6		
D_2	100% D_2	$m_{\pm1}$=176.61			2	?
(McTague *et al.*) (Ref. 34)		$m_{\pm2}$=179.17		2.56		
		m_0=181.75		2.58		
D_2	100% D_2	m_0=172.15			98.8	1.16
(Hardy *et al.*) (Ref. 16)		$m_{\pm1}$=174.75		2.6		
		$m_{\pm2}$=181.33		6.58		

the disordered lattice at 4.1 K, with the asymmetry attributed to the short-range order of J = 1 molecules. Similarly, the $S_0(1)$ line was continuous and broad for the disordered lattice, but reduced to several resolvable modes for the ordered lattice. Their interpretation of the lines was disputed by Igarashi, who claimed the libron interaction leads to a different energy structure than Hardy *et al.* predicted.[33]

3. Heteronuclear molecules

The rotational Raman spectrum of the heteronuclear molecules HD and DT is different from the homonuclear species. First, all heteronuclear molecules are in the J = 0 state in the low temperature solid because the nuclei are distinguishable. Second, the measured $S_0(0)$ line is broader for pure HD than either H_2 or D_2 with $c(1)<2\%$. McTague *et al.*[34] showed that the HD $S_0(0)$ line was composed of three polarization dependent peaks corresponding to the m_J states; however, the linewidth was about 5 cm^{-1} for each HD m_J state compared to 0.6 cm^{-1} for H_2.[30] They attributed the linewidth to lifetime broadening due to the allowed $\Delta J=1$ transitions of the heteronuclear molecules.

B. Review of vibrational raman spectra

The lowest vibrational transitions $Q_1(J)$ are Raman active modes studied extensively over the years. The vibrational energies of the J = 0 and J = 1 molecules differ slightly due to the stretching of the J = 1 molecules.[8,30] Additionally, the $Q_1(0)$ and $Q_1(1)$ energies both depend on $c(1)$,[3,35] the solid density,[9,36] and the lattice.[9,5,37]

The $Q_1(J)$ energy dependence on $c(1)$ reveals the coupling of the molecular vibrational states. The frequency shift for both density and $c(J)$ from the respective gas phase line is[8,36,38,39]

$$\Delta\nu(J)=\Delta\nu_0(J)-6\epsilon\left(\frac{V_0}{V}\right)^2 c(J), \tag{10}$$

where V is the solid molar volume, V_0 is the zero pressure solid molar volume, and $\Delta\nu_0(J)$ is the single molecule coupling. The first term in Eq. (10) is due to the isotropic interactions in the solid and the second is the vibrational coupling term. Vibrational energy bands are formed by the coupling and allow the excitation to hop to neighboring molecules. However, the coupling is only between molecules with the same J because the energy difference $\Delta Q_1 = Q_1(0) - Q_1(0)$ is nonzero.

The intensity of the $Q_1(J)$ lines are strongly dependent on $c(1)$ in pure H_2 and D_2.[3,8,38,39] There is an enhanced intensity of the lower energy $Q_1(1)$ line because, classically, the vibrating J = 1 molecule drives neighboring J = 0 molecules below their vibrational resonant frequency.[2] Thus, the $Q_1(1)/Q_1(0)$ intensity ratio is described by

$$Q_1(1)/Q_1(0)=\xi[c(1)]c(1)/c(0), \tag{11}$$

where $\xi[c(1)]$ is the concentration dependent enhancement factor.[2,38] James and Van Kranendonk initially used a coupled oscillator and interacting impurity model to calculate $\xi[c(1)]$.[2] The enhanced intensity was later successfully described by the coherent potential approximation.[39] Both models show that the small energy difference ΔQ_1 is responsible for $\xi[c(1)]>1$. The D_2 enhancement of about 50 is greater than the H_2 value of about 4 for $c(1)\approx 0$ because $\Delta Q_1 = 3.5\ \mathrm{cm}^{-1}$ for H_2 compared to $0.8\ \mathrm{cm}^{-1}$ for D_2 is smaller for D_2 than H_2.[2,38,40]

Brown and Daniels[9] found that the vibrational transition was dependent on the isotope concentration for H_2-HD-D_2 mixtures. The transitions were shifted to higher energies as the H_2 was diluted by the other isotopes by as much as 2% at about 300 kbar. Assuming that our hydrogen mixtures follow a simple scaling law, then H_2 in the H-D experiences a lattice density equivalent to 200 bar.[18] Brown and Daniels measured almost no energy shift at this pressure.

II. EXPERIMENT

Our samples consisted of a single D-T mixture and several compositions of H_2, HD, and D_2. The D-T sample was an 800 μm diameter glass shell filled with 25 atm of D-T gas at room temperature, giving 3×10^{-7} moles of D-T. The experimentally determined D-T isotopic concentration was 29-51-20 D_2-DT-T_2. The shell was glued to a sapphire window and mounted to the cold finger of a liquid helium cooled cryostat. The H_2, HD, and D_2 mixtures were deposited directly on the sapphire window. Germanium resistance thermometers monitored the cell temperature and provided feedback for the temperature controller. Temperature variations were ± 10 mK over minutes, with slow drifts of up to ± 200 mK over the course of a day. The 488 nm line of a Spectra Physics 171 Ar^+ laser excited the sample. The backscattered light was passed through a Kaiser Optical HSNF 488-1.0 holographic notch filter to remove the Rayleigh scattered light then dispersed by a Spex 1403 double monochrometer. The spectrometer gratings were 1800 lines/mm blazed for 500 nm. The Raman signal was detected with a Princeton Instruments liquid nitrogen cooled CCD camera with a 1152×256 array of 22.5-μm square pixels. $c(1)$ could not be determined below 4% in D-T because the $S_0(1)$ signal was small compared to the CCD background noise.

The pure vapor phase D_2 $S_0(0)$ transition was used to calibrate the optical system as it could be added around the D-T shell to provide an in-place calibration of the entire optical system. The spectrometer dispersion was found to be $0.21\ \mathrm{cm}^{-1}$ per pixel for the rotational lines and $0.15\ \mathrm{cm}^{-1}$ per pixel for the D_2 vibrational lines. The maximum spectrometer entrance slit width was 35 μm.

The solid was frozen quickly through the triple point and resulted in a randomly oriented multicrystalline sample. H_2, HD, and D_2 were mixed in the vapor phase, then condensed onto the substrate. The solid pressure, temperature, and $c(1)$ were such that the hcp phase is preferred for pure H_2 or D_2. However, the lattice structure was not experimentally determined for the mixtures, nor could it be inferred from the $S_0(0)$ line shape. Both $c(1)$ and the isotope ratio was determined from the relative rotational line intensities according to Eq. (2). H_2 and D_2 samples with low $c(1)$ were prepared by keeping the samples in liquid helium cooled storage beds. The J = 1-to-0 conversion took place over several weeks. It was previously shown that $c(1)$ reaches a minimum value of 0.5-1% in D-T due to beta-particle interactions.[41]

III. ROTATIONAL LINES

The rapid decay of the J = 1 population in D-T enabled a measurement of the D-T $S_0(0)$ line shapes with $c(1)$. The $S_0(J)$ lines are easily identified for each hydrogen isotope based on their respective transition energies. Thus, $c(1)_x$ and the $S_0(0)$ lines for each isotope in the mixture are readily measured. Shortly after freezing, when a significant J = 1 population exists, the D_2, T_2 and DT $S_0(0)$ lines are broad and their respective m_J components cannot be resolved, as shown in the bottom trace of Fig. 1. This observation is consistent with previous measurements of the $S_0(0)$ lines for pure component H_2 and D_2 with $c(1)\gtrsim 20\%$.[8,30] The observed lineshapes for the D-T mixture at with $c(1)\lesssim 15\%$ were not expected, and are very different from the single component results. Figure 1 shows the $S_0(0)$ lines for T_2, DT, and D_2 in D-T for decreasing $c(1)$. A triplet is evident for the T_2 $S_0(0)$ line when $c(1)_{T_2}<10\%$. However, the D_2 $S_0(0)$ line remains broad and asymmetric for $c(1)_{D_2}\lesssim 1$

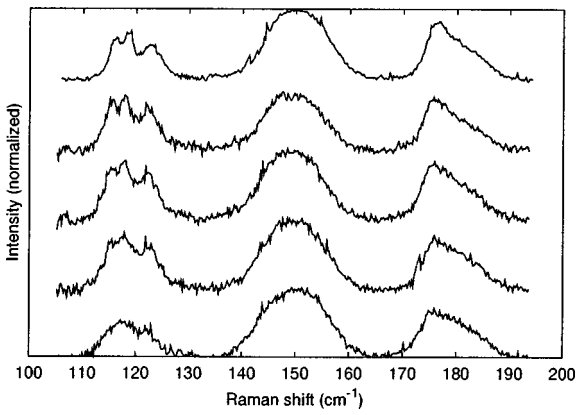

FIG. 1. The $S_0(0)$ transitions in D-T for each isotope as the J = 1 population decreases. The transitions correspond to (from left to right) T_2, DT, and D_2 molecules. The T_2 line shape is a triplet at the latest times, while the D_2 retains the asymmetric shape. The time since cooling from 77 to 6.0 K is (bottom to top) 0.4, 3.0, 6.1, and 13.2 h. The top curve was measured after 77 h at 10 K.

-2%. The DT line is broad and nearly symmetric, similar to pure HD $S_0(0)$ lines,[34] but with a few subtle differences that will be described shortly.

A. Comparison of the homonuclear isotope $S_0(0)$ transitions

D_2 was the common isotope in both the tritiated D-T and the nontritiated H-D mixtures. It is instructive to compare the D_2 $S_0(0)$ line in both mixtures to $S_0(0)$ of pure D_2. As previously described, the $S_0(0)$ m_J lines of J = 0 D_2 are split into a triplet for hcp lattice and a doublet for fcc lattice, with the triplet structure resolved when $c(1) \lesssim 20\%$.[30] However, the D_2 $S_0(0)$ triplet is not observed in D-T, even with $c(1)$ less than 2-4%. Instead, the $S_0(0)$ line has a full width at half maximum (FWHM) of 9.0 cm^{-1} and has a long, high energy tail when $c(1) < 2-4\%$. The low energy peak is less pronounced and the FWHM is 11.5 cm^{-1} with $c(1)_{D_2} = 33\%$. In contrast to D_2, the T_2 $S_0(0)$ line did split into a triplet for $c(1)_{T_2} < 10\%$. However, the T_2 triplet in D-T is not necessarily associated with the hcp lattice structure. Whereas the m_J splitting is the same to within 0.02 cm^{-1} for pure H_2 and D_2 samples,[30,34] the T_2 $S_0(0)$ lines are 2.5 and 3.9 cm^{-1} below and above the center peak respectively.

The $S_0(0)$ lines of H_2-D_2 mixtures with $c(1) < 5\%$ are shown in Fig. 2. The D_2 $S_0(0)$ line is split into the expected hcp triplet when no H_2 is present. Adding H_2 broadens the D_2 line, with the triplet becoming unresolvable when the sample contains 23% H_2. A triplet is again resolvable when the D_2 is strongly diluted by 77% H_2. Table I lists the peak positions and FWHM values for each of the $S_0(0)$ components determined by fitting $S_0(0)$ to a sum of Lorentzian lines. The FWHM of the D_2 m_J increase from 1.0 cm^{-1} for pure D_2 to 2.9 cm^{-1} and 2.5 cm^{-1} with 12% H_2. There was little observed change in the splitting of the D_2 m_J components between the 0% H_2 and 12% H_2 samples. The D_2 $S_0(0)$ line was again fit to the sum of three Lorentzian lines for 23% H_2, even though the individual lines could not be resolved, in order to obtain approximate positions and FWHM values. While the FWHM of the D_2 $S_0(0)$ components increases compared to the 0% and 12% H_2 samples, the peak positions are not significantly shifted compared to the pure component. In contrast, the D_2 $S_0(0)$ lines in the 77%H_2-23%D_2 mixture are significantly shifted in energy compared to the samples with $H_2 < 23\%$.

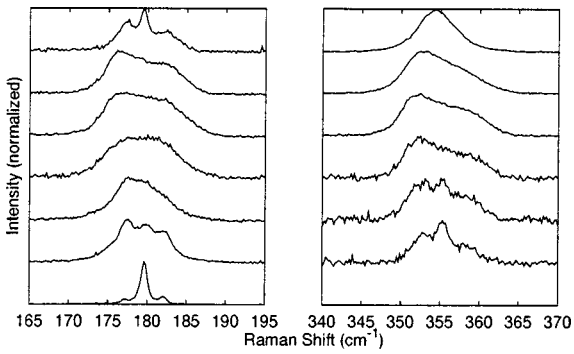

FIG. 2. The D_2 (left) and H_2 (right) $S_0(0)$ transitions for increasing H_2 concentration. The triplet structure of both isotopes is broadened as H_2 is increased. The amount of H_2 in the sample is (bottom to top) 0%, 12%, 23%, 31%, 45%, 59% and 77%.

Similarly, the H_2 $S_0(0)$ line is composed of a triplet for the lowest concentrations of H_2 in D_2, but the triplet becomes unresolvable between 23% and 31% H_2. The positions and FWHM values were again obtained by fitting to a sum of three Lorentzian lines, and are listed in Table I. As with D_2 and T_2, the H_2 $S_0(0)$ m_J components are much broader in the mixture than for pure H_2.

Next, HD was added to the H_2-D_2 mixture. The D_2 $S_0(0)$ triplet re-emerges, as shown in Fig. 3, but the lines are broad and significantly shifted in energy compared to pure D_2. The splitting of the three lines is not symmetric about the center energy, similar to the T_2 $S_0(0)$ lines in D-T. The H_2 lines do not show any evidence of a triplet, but instead have an asymmetric shape similar to that observed for D_2 in D-T. Between each step, the gas was warmed up to the vapor to ensure mixing of the hydrogens. Hence, the crystal orientation, sizes, and number are likely very different from case to case. However, the lines are qualitatively similar in all cases.

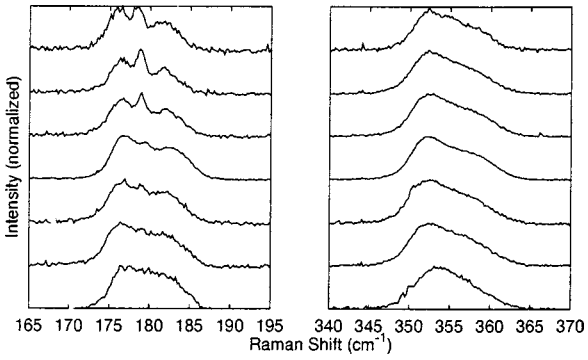

FIG. 3. The rotational lineshape for D_2 (left) and H_2 (right) as HD is added to the H_2 and D_2 mixture. The structure remains broad, but the triplet structure re-emerges. The percent of H_2-HD-D_2 is (bottom to top) 65-0-35, 55-11-34, 51-18-31, 45-27-28, 44-35-21, 46-38-16, and 29-51-20.

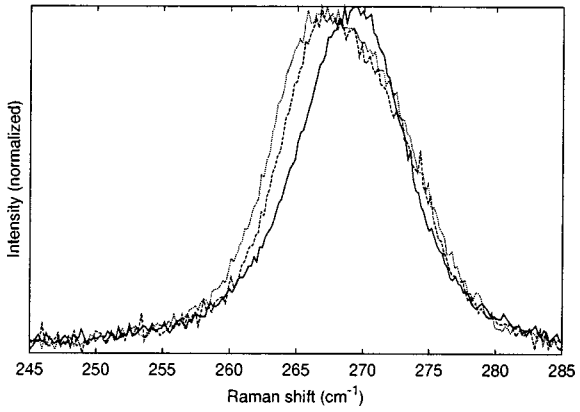

FIG. 4. The HD $S_0(0)$ line for pure HD (solid) and the H_2-HD-D_2 mixtures 45-27-28 (dashed), and 29-51-20 (dotted). The linewidth is increased in the mixtures.

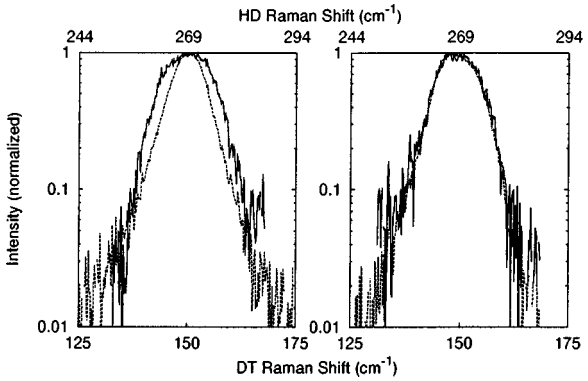

FIG. 5. The $S_0(0)$ lines for HD (dashed) and DT (solid) overlayed. The left shows pure HD with no J = 1 molecules and DT in D-T with $c(1)_{T_2}=55\%$ and $c(1)_{D_2}=30\%$. The right shows HD in H-D and DT in D-T with $c(1)_x<5\%$.

B. $S_0(1)$ in D-T

The $S_0(1)$ transition in D-T was measured for D_2 and T_2. The $S_0(1)$ line is at energy 202.5 cm^{-1} for T_2 with a FWHM of 7.5 cm^{-1}. The $S_0(1)$ line of D_2 is at 299.3 cm^{-1} and has a FWHM of 6.4 cm^{-1}. No change in energy was observed with decreasing $c(1)_{D_2}$ and $c(1)_{T_2}$. However, the D_2 $S_0(1)$ becomes narrower with decreasing $c(1)$, with low intensity wings on each side of the main peak. The $S_0(1)$ lines were not measured in the H-D samples because of the low J = 1 population in those samples.

C. $S_0(0)$ transitions of heteronuclear molecules

Figures 1 and 4 show the DT and HD $S_0(0)$ lines in their respective mixtures. There is a qualitative similarity between the two isotopes. Both are broad, symmetric transitions, not too different from previous measurements of pure component HD. Neither HD nor DT have the strong line shape changes observed for the homonuclear molecules in the mixtures. Instead, only subtle differences were noticed.

The energies and FWHM values of the DT $S_0(0)$ line as $c(1)_{D_2}$ and $c(1)_{T_2}$ decrease are listed in Table II. The FWHM increases slightly and the peak intensity shifts to higher energy as $c(1)_{T_2}$ and $c(1)_{D_2}$ increase. Similarly, the HD $S_0(0)$ line is broadened and shifted to higher energy for HD in the H-D mixture compared to pure HD. Indeed, Fig. 5 shows that the $S_0(0)$ lines of HD in H-D and DT in D-T are very nearly identical for comparable isotope ratios and $c(1)<5\%$. McTague *et al.*[34] determined the HD $S_0(0)$ line was composed of three m_J components that were each well fit by a Lorentzian line shape. Hence, they concluded that the width of the HD line was due to lifetime broadening. In contrast, HD in H-D and DT in D-T are both fit better by the sum of three Gaussian lines, suggesting that the broadening in the mixtures is due to the inhomogeneous crystalline environment.

TABLE II. Position and linewidth information of the DT $S_0(0)$ line for the D-T mixture. The linewidth decreases with decreasing $c(1)$ of D_2 and T_2.

Time after cooling (hours)	Temp. (K)	% J = 1 (D_2,T_2)	Max (cm^{-1})	Center (cm^{-1})	FWHM (cm^{-1})
0.75	11.0	(30,55)	150.9	150.7	13.5
25.5	11.0	(10,<5)	150.6	150.25	12.4
77.0	10.2	(<4,<4)	150.0	150.0	12.6

D. Rotational line shape discussion

The matrix of the mixtures differs from the single component case in three ways that alter the $S_0(0)$ transitions. First, each isotope has a different rotational energy due to their differing masses. Second, the interaction potential varies slightly with the isotope. Finally, the lattice is distorted from the ideal hcp structure by the different sized molecular wave functions. The following discussion assumes only molecules in the $\nu=0$ vibrational state on a rigid lattice.

The J = 2 excitation of a D_2 molecule cannot hop to a neighboring H_2 molecule because the two have different rotational energies. Thus, the allowed rotational band states due to the EQQ interaction in a mixed hydrogen lattice are not the same as the single component case. New rotational states are accessible in the mixed lattice, and this broadens the $S_0(0)$ transition. The crystal field terms of Eq. (7) are similarly altered, most notably for the distorted hcp lattice. While the small numbers of rotons in the lattice at any given time do not interact with each other, they each sample a different local lattice configuration. Hence, the measured $S_0(0)$ line is an ensemble average of many different band energies. Thus the fact that the $S_0(0)$ triplet broadens in mixtures of the hydrogens is not surprising. The origin of the $S_0(0)$ triplet for the low concentration homonuclear isotope in H-D or D-T mixtures can also be explained in terms of the altered band energies, as described below.

The calculation in Sec. I A was modified to numerically model the mixed H_2-D_2 matrix with varying H_2 concentration. Only the EQQ hopping interaction was calculated for the mixed lattice. In the model, H_2 and D_2 molecules are randomly placed, based on the desired H_2 concentration, at specific lattice sites of a perfect lattice. The EQQ coupling

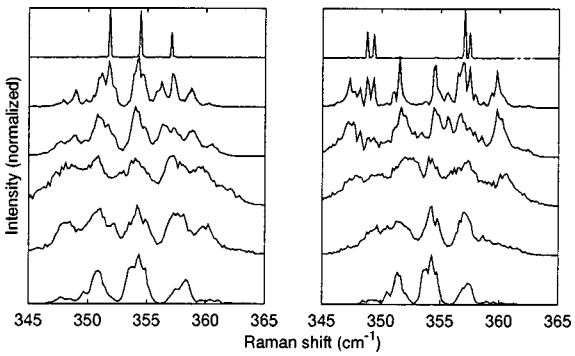

FIG. 6. Calculated spectrum for the $S_0(0)$ line of H_2 in an H_2-D_2 lattice for hcp (left) and fcc (right) lattice structures. The H_2 concentrations are (bottom to top) 12%, 30%, 50%, 80%, 90%, and 100%.

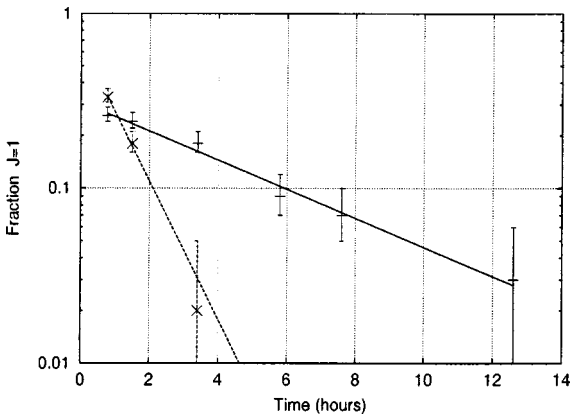

FIG. 7. Measured T_2 ($\times$) and D_2 ($+$) $c(1)$ vs time at 8.1 K. The J = 1 concentrations for both isotopes decay exponentially. The straight lines are least squares fits to the data.

strength ϵ_{02} is dependent on the nearest neighbor distance, which was linearly interpolated from the pure D_2 3.605-Å to the pure H_2 3.789-Å values based on the H_2 concentration. The lattice sum in Eq. (5) is taken only over lattice sites which have the same isotope as the molecule at the origin since the excitation cannot hop to molecules with difference $S_0(0)$ energies. The energy eigenvalues are found by diagonalizing the resulting matrix in Eq. (3). The eigenvalues are then averaged for many randomly generated configurations to approximate the spectrum observed in a real crystal. The resulting spectra for H_2 are presented, with D_2 qualitatively the same. The polarization dependence of the intensity was neglected so that we report only the allowed energy spectrum. The interactions were calculated only to molecules within 5 nearest neighbors of the central molecule. Going further did not significantly alter the results for the cases tested.

The calculated H_2 $S_0(0)$ spectra for the hcp and fcc lattices are shown in Fig. 6 for several H_2 concentrations. Concentrations of less than about 5% (not shown) reduce to a single line with no energy shift from the free molecule value because there are, on average, no nearest neighbor pairs of H_2 molecules. The hcp and fcc $S_0(0)$ lines are split into nearly identical triplets at 12% H_2 concentration. The $S_0(0)$ transition remains broad for H_2, less than 90%, finally recovering the familiar hcp triplet and fcc doublet at 100%. The calculated spectrum will be further broadened by the crystal field terms. While the calculation does not exactly match the experiment, it does reproduce the more striking features. This indicates the $|2m\rangle$ states are mixed in the H_2-D_2 lattice, and m is no longer a good quantum number. Therefore, the individual components of the T_2 triplet in D-T and the D_2 triplet in H-D are not designated by m_J. Including crystal field terms and distortions from the perfect lattice in the calculation will further modify the spectra, tending to broaden the transition, and will likely lead to the observed difference between Δ_1 and Δ_2.

Thus, the $S_0(0)$ triplet for hydrogen mixtures is not unique to the hcp lattice, and the crystal structure of the D-T and H-D mixtures remains uncertain. Furthermore, the H-D and D-T mixtures are qualitatively similar, hence there is no observable effect of radiation damage or free atoms on the rotons.

E. J = 1-to-0 conversion rates

The J=1-to-0 transition of H_2 and D_2 molecules is a second order process in $c(1)$. The magnetic dipole-dipole (and electric quadrupole-quadrupole for D2) interaction of neighboring J = 1 molecules flips the spin of one of the nucleons with a simultaneous change in rotational state. The J = 1-to-0 conversion in D-T was found to be dominated by the atoms created by the tritium radioactivity.[21,42–44] The diffusion of atoms through the solid leads to a first order conversion rate in the D-T mixture. The very large electric field of the atoms and electrons created by the triton beta decay and subsequent ionization is responsible for the rapid conversion. Furthermore, the difference in conversion rates for D_2 and T_2 was attributed to their different magnetic moment, consistent with the theory. However, the NMR measurements were an indirect measure of the D_2 J = 1 populations in the sample. The rotational Raman spectrum was used to obtain the relative number of molecules in each rotational state.

Figure 7 shows $c(1)_x$ for T_2 and D_2, determined according to Eq. (2), as a function of time at 8.1 K. $c(1)_x$ decays exponentially in time for both isotopes, in agreement with the hopping model, and in contradiction to the second order process of natural conversion. Table IV shows the measured time constants at a series of temperatures. The typical error is ± 0.3 h for $\tau(T_2)$ and 0.6 h for $\tau(D_2)$. The average $\tau(D_2)/\tau(T_2)$ ratio is 3.7 h for all measurements between 5 and 10 K, in close agreement with the expected ratio of 3.47 based on the D_2 and T_2 magnetic moment ratios.

TABLE III. Position and linewidth information of the HD $S_0(0)$ line for mixtures of HD, H_2, and D_2.

Sample H_2-HD-D_2	Temp. (K)	Max (cm^{-1})	Center (cm^{-1})	FWHM (cm^{-1})
1-98-1	8.2	269.1	269.1	9.4
45-27-28	6.5	267.1	268.1	11.0
29-51-20	7.8	267.0	268.4	11.9

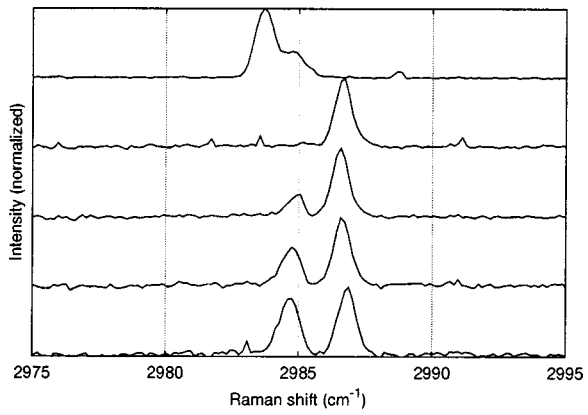

FIG. 8. $Q_1(1)$ (left) and $Q_1(0)$ (right) of D_2 in D-T for $c(1)_{D_2}$ (bottom to top) 30%, 19%, 10%, $<2\%$. The top spectrum is pure D_2 with 4% J=1. The sample temperature was 8.0 K.

IV. VIBRATIONAL LINES

The $Q_1(0)$ and $Q_1(1)$ Raman transitions were recorded for the isotopes in the D-T and H-D mixtures. The instrument resolution of ≈ 0.16 cm^{-1}/pixel is much larger than the vibron intrinsic FWHM of 0.002 cm^{-1} for $c(1)=1.3\%$ H_2.[39] Vapor and solid phase D_2 $Q_1(J)$ lines with $c(1)<1\%$ served to calibrate the spectrometer energies. Thus, the relative energy shifts and difference $\Delta Q_1 = Q_1(0) - Q_1(1)$ are known more accurately than the absolute energies, especially for H_2 and T_2. $Q_1(J)$ energies and intensities were obtained by fitting the measured lines to a Gaussian function.

A. $Q_1(J)$ energies in D-T and H-D mixtures

Figures 8 and 9 show typical D_2 and T_2 $Q_1(J)$ transitions in D-T. $Q_1(0)$ is the higher energy line in each of the figures. $c(1)_{T_2}$ and $c(1)_{D_2}$ were calculated using the time constants obtained in Table III. The T_2 time constant is shorter than D_2, thus the observed changes in the T_2 $Q_1(J)$ are not strongly influenced by $c(1)_{D_2}$, and vice versa. ΔQ_1 is small for both D_2 and T_2 and in many cases at the limit of our resolution. ΔQ_1 decreases with decreasing $c(1)_x$ for both D_2 and T_2, shown in Fig. 10. The straight lines in the figure are linear least squares fits to the data, with

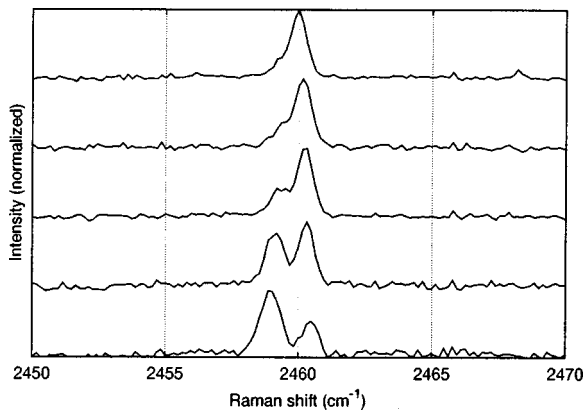

FIG. 9. $Q_1(1)$ (left) and $Q_1(0)$ (right) of T_2 in D-T for $c(1)_{T_2}$ (bottom to top) 50%, 23%, 8%, 3%, $<1\%$. The sample temperature was 8.0 K.

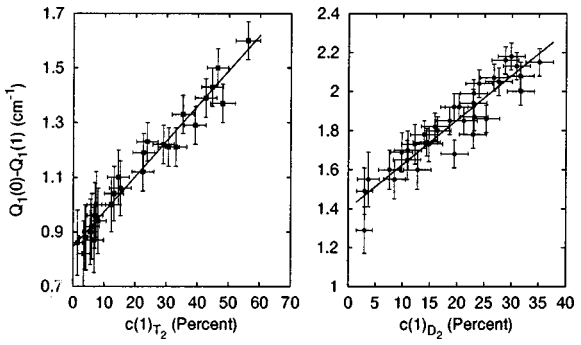

FIG. 10. Energy difference ΔQ_1 for T_2 (left) and D_2 (right) in D-T as a function of $c(1)$. The separation decreases as J = 1 decreases. The straight lines are linear least square fits to the data described in the text.

$$\Delta Q_1 = \begin{cases} 0.84 + 0.013 c(1)_{T_2} & T_2 \\ 1.40 + 0.023 c(1)_{D_2} & D_2 \end{cases}. \tag{12}$$

ΔQ_1 is smaller for T_2 than D_2 at a given $c(1)_x$, consistent with the isotope change previously observed with D_2 and H_2.[3,39,40] Figure 8 includes the $Q_1(J)$ lines in pure D_2 with $c(1)_{D_2} \approx 4\%$, and shows that the D_2 $Q_1(0)$ line is shifted higher by 1.9 cm^{-1} in D-T with low $c(1)_{D_2}$ than in pure D_2. Similarly, ΔQ_1 is larger for D_2 in D-T than for pure D_2.

Corresponding shifts in the D_2 $Q_1(J)$ energies were found as H_2 and D_2 were mixed as shown in Fig. 11. $c(1)_{D_2} = 4\%$ and $c(1)_{H_2} = 6\%$ for each plot in Fig. 11. The $Q_1(J)$ energies are plotted in Fig. 12 as a function of D_2 concentration, where the mixture included HD for points with less than 39% D_2. The linear fits in Fig. 12 are

$$\begin{aligned} Q_1(0) &= 2987.5 - 0.027 c_{D_2} \\ Q_1(1) &= 2985.8 - 0.015 c_{D_2}. \end{aligned} \tag{13}$$

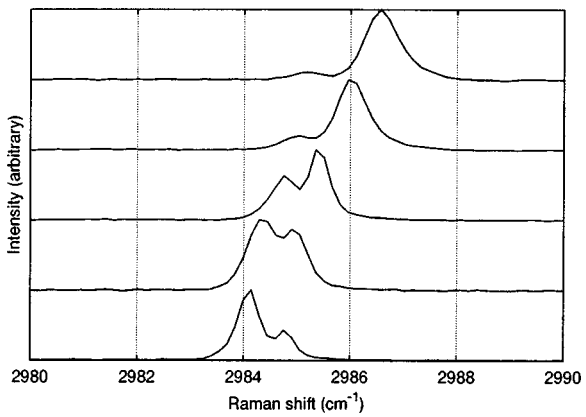

FIG. 11. The D_2 vibrational spectrum as H_2 is mixed with D_2. The amount of H_2 is (bottom to top) 0%, 12%, 31%, 45%, and 59%. $c(1)_{D_2} < 5\%$.

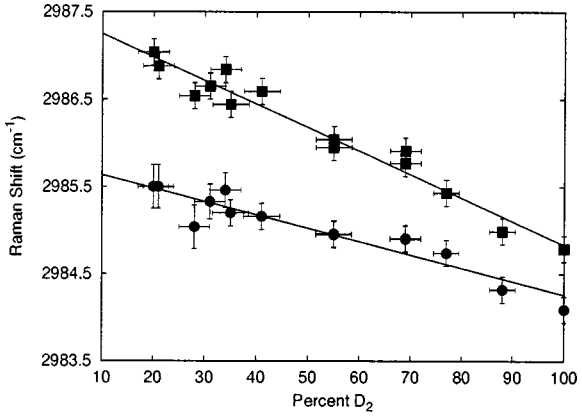

FIG. 12. The energy shift of the D_2 $Q_1(1)$ (●) and $Q_1(0)$ (■) as H_2 and HD are added.

The fits do not depend on whether the mixture is H_2-D_2 or H_2-HD-D_2. Furthermore, the D_2 $Q_1(J)$ lines in H-D are at nearly the same energy for equivalent $c(1)_{D_2}$ and D_2 concentrations in D-T. Thus, the energy shift of D_2 $Q_1(J)$ lines depends only on the D_2 concentration and not on the components of the mixture.

The H_2 lines were recorded with the addition of HD to the mixture. A small increase of $\Delta Q_1 = 4.66$ cm^{-1} to 5.00 cm^{-1} was found when the H_2 concentration decreased from 65% to 44%. The H_2 $Q_1(1)$ line consisted of a doublet separated by 0.5 cm^{-1} in energy, previously attributed to clustering of J = 1 molecules.[38]

B. $Q_1(1)/Q_1(0)$ intensity ratio in D-T and H-D

Figure 13 shows the measured $Q_1(1)$ to $Q_1(0)$ intensity ratio for two cases. The first shows the increase of $Q_1(1)/Q_1(0)$ with $c(1)_x$ for D_2 and T_2 in D-T. The fit functions are

$$Q_1(1)/Q_1(0) = \begin{cases} 2.19\,\dfrac{c(1)_{T_2}}{100-c(1)_{T_2}} + 0.28 & T_2 \\ 2.29\,\dfrac{c(1)_{D_2}}{100-c(1)_{D_2}} & D_2 \end{cases}. \quad (14)$$

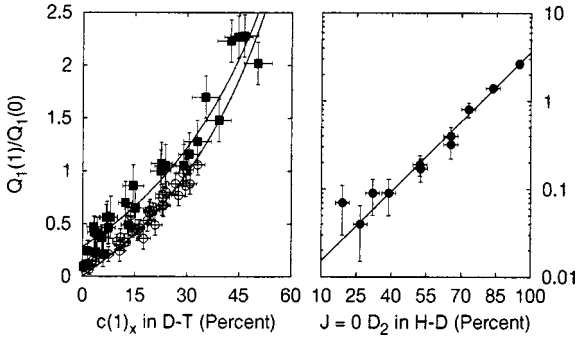

FIG. 13. Ratio of the $Q_1(1)$ to $Q_1(0)$ intensities. Left is for T_2 vs $c(1)_{T_2}$ (squares) and D_2 vs $c(1)_{D_2}$ (open circles) in D-T. Right is D_2 concentration (solid circles) of the H_2-HD-D_2 mixture. The lines are fits to the data as described in the text.

The first term is the concentration ratio multiplied by the enhancement factor, ξ in Eq. (11). Thus, the intensity ratio is enhanced by more than a factor of two for both D_2 and T_2 in the D-T mixture. The fit does not pass through the origin for T_2 which may indicate the calculated $c(1)_{T_2}$ is low by 3–4 %.

The second plot in Fig. 13 shows an exponential increase of the intensity ratio with D_2 concentration in the H-D mixture with $c(1)_{D_2} = 4\%$. The fit function is

$$Q_1(1)/Q_1(0) = 8.4\times 10^{-3}\exp[c(0)_{D_2}/16.5]. \quad (15)$$

These results show that ξ is slightly higher for D_2 in D-T than D_2 in H-D under equivalent conditions. Both mixtures have ξ's for D_2 which are much lower than is found in the pure component for a given $c(1)_{D_2}$.

C. Discussion

A common point in both D-T and H-D mixtures is when they each have 30% D_2 and $c(1)_{D_2} \approx 5\%$. The D_2 $Q_1(0)$ line is at 2986.7 cm^{-1} in both mixtures, while the $Q_1(1)$ line is at 2985.2 cm^{-1} in D-T and 2985.35 cm^{-1} in H-D. Both lines are shifted substantially from the pure D_2 with $c(1)_{D_2} = 5\%$ values of $Q_1(0) = 2984.8$ cm^{-1} and $Q_1(1) = 2983.7$ cm^{-1}. It is important to note that the solid density is lower (higher) for H-D (D-T) than D_2 at zero pressure and equivelent temperatures. Rather, the energy shift depends only on the D_2 concentration. The $Q_1(0)$ shift with increasing impurity concentration is consistent with Eq. (10) where $c(J=0)$ is replaced by the D_2 concentration. The predicted shift for D_2 $Q_1(0)$ is 1.6 cm^{-1} using $6\epsilon = 2.2$ cm^{-1} with 30% D_2, close to the 1.9 cm^{-1} found in the experiment. In contrast, $Q_1(1)$ is not expected to shift appreciably with the addition of H_2 and HD based on Eq. (10). The absolute D_2 J = 1 concentration decreases from 4% to 1.2% when D_2 is diluted to 30% of the sample. The initial sample with $c(1)_{D_2} = 4\%$ would show an energy increase of 0.1 cm^{-1} using Eq. (10) instead, of the 1.05 cm^{-1} actually measured.

Clustering of J = 1 molecules[38] is one possible explanation for the $Q_1(1)$ line shift. However, the J = 1 molecules in the initial sample had on average 0.5 J = 1 nearest neighbors, and should be dominated by clusters of number $n=0$ and 1. The energy difference of the $n=0$ and 1 clusters needs to be about 1 cm^{-1} to explain the data, larger than the 0.4 cm^{-1} found for H_2 (Ref. 38) and 0.2 cm^{-1} for D_2.[40] Furthermore, a splitting of the required magnitude is not found for D_2 in D-T for any $c(1)_{D_2}$ value. While clustering likely exists, the individual components cannot be resolved in the data.

The dependence on D_2 concentration but not the other isotopes suggests that reduced lattice symmetry is responsible for the vibron energy shift. The vibrons cannot hop between different isotopes, thus altering the band states of the crystal and shifting the $Q_1(J)$ lines.[45] This explanation is supported by a comparison with liquid D_2. Bhatnagar *et al.* found that the $Q_1(1)$ and $Q_1(0)$ lines in liquid D_2 are higher by 1.7 and 1.4 cm^{-1}, respectively, compared to the solid.[30]

TABLE IV. Measured 1/e times for T_2 and D_2 $J=1\rightarrow 0$ in this experiment.

Temp. (K)	$\tau(T_2)$ (hours)	$\tau(D_2)$ (hours)	$\tau(D_2)/\tau(T_2)$
5.4	6.1	9.1	1.5
5.4	1.5	5.3	3.5
5.8	1.7	5.9	3.5
6.0	2.8	9.1	3.2
6.7	2.4	5.3	2.2
7.2	2.2	8.3	3.8
7.2	2.4	6.8	2.8
7.2	1.5	6.9	4.6
8.1	1.1	5.2	4.7
8.2	1.9	6.1	3.2
8.6		7.5	
8.7	1.5	7.3	4.9
9.3	2.0	8.8	4.4
9.6	2.2	6.2	2.8
9.6	1.9	7.8	4.1
10.2	1.1	7.6	6.9
10.2	1.8	8.8	4.9
10.2		5.8	
10.8	1.1	15.5	14
11.3	3.3	22	6.6
11.7	5.3	30	5.7

The magnitude of the shift is consistent with our measurement, even though their data was for $c(1)_{D_2}=20\%$.

The coupling of the J = 1 and 0 vibrons leads to the enhanced $Q_1(1)/Q_1(0)$ ratio in the hydrogens, as discussed in Sec. I B, compared to the $c(1)/c(0)$ ratio. ξ is less in the D-T and H-D mixtures than in the pure components. The coupling between different isotopes is very weak because of the very large energy difference between their vibrational states.[2,39,40] Thus, ξ is reduced in mixtures because the there are fewer neighboring molecules with strong coupling (see Tables IV and V).

V. CONCLUSIONS

Rotational and vibrational Raman spectra of hydrogen mixtures are very different from the pure components. Both rotons and vibrons are localized in the mixture by the isotopic energy difference of the respective transitions. The well defined spatial symmetry of the hcp lattice is lost and the $S_0(0)$ m_J states are broadened into a continuous band. Thus, the hcp and fcc lattices cannot be distinguished in mixtures using the Raman spectra, as can be done with pure components. The vibron localization in mixtures increases the $Q_1(J)$ energy in the solid mixtures by nearly the same amount observed in the pure-component liquid. Similarily, the $Q_1(1)/Q_1(0)$ intensity enhancement for a given isotope is reduced in the mixtures compared to the pure component.

TABLE V. Measured $Q_1(0)$ and $Q_1(1)$ line positions for H_2, D_2, and T_2.

Species	Temp. (K)	$Q_1(0)$ (cm^{-1})	$Q_1(1)$ (cm^{-1})	ΔQ_1 (cm^{-1})
H_2 in 75 % J = 1 H_2 solid	8.2	4151.5	4142.8	8.7
44-35-21 H_2-HD-D_2	7.2	4150.2	4145.2	5.0
65-0-35 H_2-HD-D_2	8.5	4149.6	4145.0	4.6
D_2 in D_2 vapor $<1\%$ J=1	25	2993.5		
D_2 in 5% J = 1 D_2 solid	8	2984.8	2983.7	1.1
D_2 in $<1\%$ J = 1 D_2 solid	12.7	2984.8	2984.1	0.7
D_2 in 30% J = 1 D-T solid	8	2986.9	2984.7	2.2
D_2 in J = 0 D-T solid	8	2986.7	2985.2	1.5
D_2 in J = 0 59% H_2	9.5	2986.6	2985.4	1.2
D_2 in J = 0 31% H_2	8	2985.4	2984.8	0.6
D_2 in J = 0 12% H_2	9	2984.9	2984.3	0.6
T_2 in 50% J = 1 D-T solid	8	2460.5	2458.9	1.6
T_2 in J = 0 D-T solid	8	2460.0	2459.2	0.8

D_2 was common to all mixtures studied and showed that the $S_0(0)$ and $Q_1(J)$ spectra were nearly identical in H-D and D-T with similar D_2 and J = 1 concentrations. The spectra depend only on the D_2 concentration, not the other components of the mixture. Finally, neither the $S_0(J)$ nor the $Q_1(J)$ lines appear to be effected by radiation damage in our D-T sample. The D-T lines are qualitatively similar to the H-D lines, and appear to depend on the mixture concentration, but not the actual impurity molecules in the mixture. The only radiation effect was the previously observed enhanced J = 1-to-0 conversion rate.

ACKNOWLEDGMENTS

This work was performed under the auspices of the U.S. Department of Energy by the University of California, Lawrence Livermore National Laboratory under Contract No. W-7405-Eng-48.

[1] J. V. Kranendonk and V. F. Sears, Can. J. Phys. **44**, 313 (1966).
[2] H. M. James and J. V. Kranendonk, Phys. Rev. **164**, 1159 (1967).
[3] W. R. C. Prior and E. J. Allin, Can. J. Phys. **50**, 1471 (1972).
[4] W. R. C. Prior and E. J. Allin, Can. J. Phys. **51**, 405 (1973).
[5] M. E. Alikhani, B. Silvi, J. P. Perchard, and V. Chandrasekharan, J. Chem. Phys. **90**, 5221 (1989).
[6] V. Chandrasekharan, M. Chergui, B. Silvi, and R. D. Etters, J. Phys. Chem. **91**, 1623 (1987).
[7] B. Silvi, V. Chandrasekharan, M. Chergui, and R. D. Etters, Phys. Rev. B **33**, 2749 (1986).
[8] J. V. Kranendonk, *Solid Hydrogen* (Plenum Press, New York, 1983).
[9] D. M. Brown and W. B. Daniels, Phys. Rev. A **45**, 6429 (1992).
[10] I. F. Silvera and R. J. Wijngaarden, Phys. Rev. Lett. **47**, 39 (1981).
[11] F. Moshary, N. H. Chen, and I. F. Silvera, Phys. Rev. B **48**,

12 613 (1993).
[12] J. V. Kranendonk, Can. J. Phys. **38**, 240 (1960).
[13] I. F. Silvera, Rev. Mod. Phys. **52**, 393 (1980).
[14] J. Lindl, Phys. Plasmas **2**, 3933 (1995).
[15] K. Veirs, Tech. Rep. LBL-20565, Lawrence Berkeley Laboratory, 1985.
[16] W. N. Hardy, I. F. Silvera, and J. P. McTague, Phys. Rev. B **12**, 753 (1975).
[17] M. C. Drake, G. J. Rosasco, R. Schneggenburger, and R. L. Nolen, Jr., J. Appl. Phys. **50**, 7894 (1979).
[18] P. C. Souers, *Hydrogen Properties for Fusion Energy* (University of California Press, Berkeley, 1986).
[19] G. W. Collins, P. C. Souers, J. L. Maienschein, E. R. Mapoles, and J. R. Gaines, Phys. Rev. B **45**, 549 (1992).
[20] J. R. Gaines, P. A. Fedders, G. W. Collins, J. D. Sater, and P. C. Souers, Phys. Rev. B **52**, 7243 (1995).
[21] J. D. Sater, J. R. Gaines, E. M. Fearon, P. C. Souers, F. E. McMurphy, and E. R. Mapoles, Phys. Rev. B **37**, 1482 (1988).
[22] J. J. Miller, R. L. Brooks, and J. L. Hunt, Can. J. Phys. **71**, 501 (1993).
[23] K. Motizuki and T. Nagamiya, J. Phys. Soc. Jpn. **11**, 93 (1956).
[24] K. Motizuki, J. Phys. Soc. Jpn. **12**, 1192 (1962).
[25] J. A. Berlinsky and W. N. Hardy, Phys. Rev. B **8**, 5013 (1973).
[26] W. Kolos and L. Wolniewicz, J. Chem. Phys. **46**, 1426 (1968).
[27] C. Schwartz and R. J. Le Roy, J. Mol. Spectrosc. **121**, 420 (1987).
[28] S. C. Durana and J. P. McTague, Phys. Rev. Lett. **31**, 990 (1973).
[29] J. V. Kranendonk and G. Karl, Rev. Mod. Phys. **40**, 531 (1968).
[30] S. S. Bhatnagar, E. J. Allin, and H. L. Welsh, Can. J. Phys. **40**, 9 (1962).
[31] E. Goovaerts, X. Y. Chen, A. Bouwen, and D. Schoemaker, Phys. Rev. Lett. **57**, 479 (1986).
[32] M. Leblans, A. Bouwen, C. Sierens, W. Joosen, E. Goovaerts, and D. Schoemaker, Phys. Rev. B **40**, 6674 (1989).
[33] J. Igarashi, Prog. Theor. Phys. **61**, 719 (1979).
[34] J. P. McTague, I. F. Silvera, and W. N. Hardy, in *Light Scattering in Solids: Proceedings of the Second International Conference on Light Scattering in Solids*, edited by M. Balkanski (Flammarion Sciences, Paris, 1971), pp. 456–459.
[35] W. R. C. Prior and E. J. Allin, Can. J. Phys. **51**, 1935 (1973).
[36] E. J. Allin and S. M. Till, Can. J. Phys. **57**, 442 (1979).
[37] H. Kreek and R. J. Le Roy, J. Chem. Phys. **63**, 338 (1975).
[38] V. Soots, E. J. Allin, and H. L. Welsh, Can. J. Phys. **43**, 1985 (1965).
[39] J. De Kinder, A. Bouwen, D. Schoemaker, A. Boukahil, and D. L. Huber, Phys. Rev. B **49**, 12 754 (1994).
[40] J. De Kinder, A. Bouwen, D. Schoemaker, A. Boukahil, and D. L. Huber, Phys. Rev. B **49**, 12 762 (1994).
[41] G. W. Collins, P. C. Souers, J. L. Maienschein, E. R. Mapoles, and J. R. Gaines, Phys. Rev. B **45**, 549 (1992).
[42] Y. Cao, J. R. Gaines, P. A. Fedders, and P. C. Souers, Phys. Rev. B **37**, 1474 (1988).
[43] G. W. Collins, E. M. Fearon, E. R. Mapoles, R. T. Tsugawa, P. C. Souers, and P. A. Fedders, Phys. Rev. B **44**, 6598 (1991).
[44] G. W. Collins, E. M. Fearon, E. R. Mapoles, R. T. Tsugawa, P. C. Souers, and P. A. Fedders, Phys. Rev. B **46**, 695 (1992).
[45] J. L. Feldman, J. H. Eggert, J. De Kinder, H. K. Mao, and R. J. Hemley, J. Low Temp. Phys. **115**, 181 (1999).